Neural Field Description Suggests Feedforward Mechanism of State-Dependent Visual Receptive Field Changes

Katrin Suder[1]*, Florentin Wörgötter[1], and Thomas Wennekers[2]

[1]Institute of Physiology, Dept. of Neurophysiology,
Ruhr-University, D-44780 Bochum, Germany
Email: suder@neurop2.ruhr-uni-bochum.de

[2]Dept. of Neural Information Processing
University of Ulm, D-89069 Ulm, Germany
Email: thomas@neuro.informatik.uni-ulm.de

Abstract

Cortical receptive fields have recently been shown to be wider during synchronized than during non-synchronized EEG states, where, in addition, they can shrink over time in response to flashed stimuli. In the present paper we employ a neural field approach to describe the cortical activity patterns analytically. Expressions for spatio-temporal receptive fields are derived and fitted against experimental data. The model supports the idea that the observed receptive field restructuring is mainly driven by state-dependent LGN firing patterns (burst vs. tonic mode).

1 Introduction

Receptive field sizes in the primary visual cortex (V1) have recently been shown to depend on the state of the Electroencephalogram (EEG) [12]. In synchronized states (dominated by $\alpha-$ or $\delta-$waves) they are significantly wider than in less or non-synchronized states ($\beta-$EEG). In addition their width can considerably shrink over time in response to flashed light spots during non-synchronized states (Fig.1C and [12]). Different LGN firing patterns during different EEG states have been suggested as the main mechanism for this restructuring [12]. During synchronized EEG, LGN cells respond to visual stimuli mainly with a contrast independent phasic burst of spikes at high frequency (Fig.1A). These bursts are strong enough to drive cortical cells also further away from the main projection column, whereby they evoke wide receptive fields. In contrast, during non-synchronized states, the burst component is often diminished. Instead, LGN cells respond with a long-lasting tonic firing pattern at much lower (and contrast dependent) rates (Fig.1B). Accordingly, one expects a transient and relatively broad initial receptive field (due to the burst) which sharpens quickly (due to the tonic component) just as observed experimentally (Fig.1C).

The above hypothesis has been tested by means of biologically detailed computer simulations [12]. The present paper takes a more abstract level of description in form of neural field equations [1, 7, 11]. Those enable an analytical derivation of the spatio-temporal cortical activity, the explicit time-dependence of the receptive field width, and first firing times of differently strongly excited neurons. Moreover, cortical parameter sets can be obtained by fitting the model against experimental data.

2 Theory

The cortical layer V1 is idealized by a one-dimensional array of cells [1, 6, 7, 11]. V1 receives input from LGN whereas lateral and feedback connections are neglected. Those had been implemented in our earlier large

*Acknowledgements: K.S. and F.W. acknowledge support of the DFG and of the HFSP. T.W. was supported by DFG grant Pa 268/8-1. The authors would like to thank K. Funke (Bochum) and H.E. Plesser (Göttingen) for valuable comments and discussions.

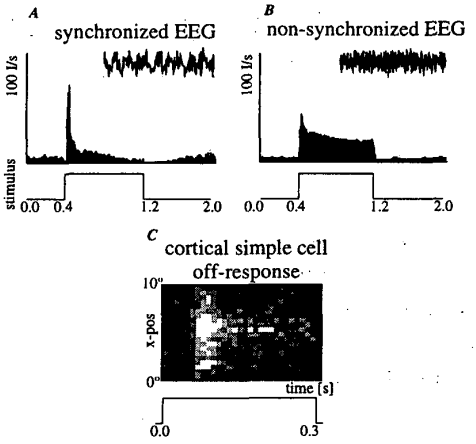

Fig.1: A,B: Peri-stimulus-time histograms of visual responses of an LGN relay cell during different EEG states in an anesthetized cat. The stimulus in form of a small light dot was on between 0.4 s and 1.2 s. Note that in both EEG states, the neural response starts with bursting. Parts (5 s) from EEG-traces are shown in the insets. C: Shrinking of receptive field width of a cortical cell with latency after stimulation, recorded during the non-synchronized EEG. The total number of spikes is grey-scale coded (0-40 I/s).

scale simulations [12], but their influence was not essential for the main mechanisms of state-dependent receptive field sharpening. Therefore, the neural activity in V1, ϕ, can be written as a spatio-temporal convolution with the LGN input, $I(x,t)$:

$$\phi(x,t)=\int_0^t\int_{-\infty}^{\infty} g(t-t')K(x-x')I(x',t')dx'dt' \quad (1)$$

The kernel $g(t)$ in (1) describes the cortical temporal response function and $K(x)$ the feedforward projections from LGN to cortex. We choose

$$g(t) = \frac{1}{\tau}\, e^{-t/\tau} \text{ and } K(x) = \frac{K_0}{\sqrt{2\pi}}\, e^{-\frac{x^2}{2\sigma_0^2}} \quad (2)$$

Thus, the temporal cortical dynamics is assumed to follow a first order low pass dynamics with time-constant τ. In assuming a Gaussian connectivity profile for $K(x)$ we restrict our considerations to single on- or off-subfields. Receptive fields consisting of several subfields can be modeled by superpositions of several responses of the form (1) with appropriate g and K. The factor $K_0/\sqrt{2\pi}$ in (2) plays the role of an effective synaptic strength.

In a first approximation, we assume that the input from LGN to V1 is separable in space and time: $I(x,t) = I_x(x)I_t(t)$ (cf. [3, 7]) and can be expressed by phenomenological activity functions. Experimental stimuli in [12] are small light spots. Those evoke localized activity profiles in the LGN, which are represented in our model by a Gaussian function $I_x(x)$, Eqn. (3). The temporal component $I_t(t)$ of the LGN activity is modeled by the phenomenological activity functions (4) and (5), which already contain the state-dependence and approximate the experimentally observed LGN firing patterns (Fig. 1A,B):

$$I_x(x) = e^{-\frac{x^2}{2\sigma_1^2}} \quad (3)$$

$$Is_t(t) = c_1\Theta(t)\Theta(t_1 - t) \quad (4)$$

$$Ins_t(t) = Is_t(t) + c_2\Theta(t - t_1)\Theta(t_2 - t) \quad (5)$$

In (4) and (5), $\Theta(t)$ is the Heaviside function. $Is_t(t)$ describes the high-frequency burst of spikes in the synchronized EEG in form of a rectangular pulse of strength c_1 lasting from $t = 0$ to t_1. The bursts are due to intrinsic LGN membrane properties (low-threshold Ca-bursts) and the interplay with inhibitory PGN neurons, modeled in more detail in [12]. $Ins_t(t)$ contains the additional tonic component of height $c_2 < c_1$ lasting from t_1 to t_2.

We are now ready to compute the cortical spatio-temporal activity profile $\phi(x,t)$. Because we assumed stimulation by small light spots, this profile can be interpreted as the cortical point spread function or, in light of the linearity and spatial homogeneity of the model, as the spatio-temporal receptive field of our model cells. Inserting the assumptions (2)–(5) into (1), one observes that the cortical response separates into a spatial component $X(x)$ and a temporal component $T(t)$, that is $\phi(x,t) = X(x)T(t)$. The integrals for X and T, however, can be solved analytically. $X(x)$ is a convolution of two Gaussians, the input distribution $I_x(x)$ and the feedforward kernel $K(x)$:

$$X(x) = \frac{K_0\sigma_0\sigma_1}{\sigma_r}\, e^{-\frac{x^2}{2\sigma_r^2}} \approx K_0\sigma_1\, e^{-\frac{x^2}{2\sigma_0^2}} \quad (6)$$

where $\sigma_r^2 := \sigma_0^2 + \sigma_1^2$ and the approximation holds for small stimuli, $\sigma_1 \ll \sigma_0$.

For the temporal factor $T(t)$ one gets three different regimes $t_0 \le t < t_1$, $t_1 \le t <$

t_2, and $t_2 \leq t$. t_0 accounts for latencies between stimulus onset and cortical response. Setting $\Delta c := c_1 - c_2$ for the difference between burst and tonic firing, this leads to the following term for the non-synchronized state (5)

$$T(t) = \begin{cases} c_1(1 - e^{-\frac{t-t_0}{\tau}}) \\ c_2 - c_1 e^{-\frac{t-t_0}{\tau}} + \Delta c e^{-\frac{t-t_1}{\tau}} \\ c_2 e^{-\frac{t-t_2}{\tau}} - c_1 e^{-\frac{t-t_0}{\tau}} + \Delta c e^{-\frac{t-t_1}{\tau}} \end{cases} \quad (7)$$

The synchronized response $T(t)$ is obtained from (7) by setting $c_2 = 0$. A typical cortical response $\phi(x,t) = X(x)T(t)$ in the non-synchronized state is shown in Fig. 2 and should be compared with Fig. 1C. It can be seen that the membrane potential quickly increases to its maximum value during the burst phase and afterwards declines to the value of the tonic component.

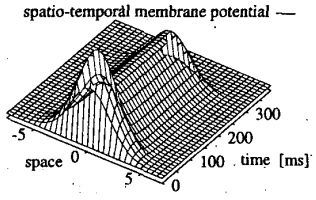

Fig.2: Cortical potential $\phi(x,t)$ for the non-synchronized case with the following parameters: $\sigma_0 = 1.7$, $\sigma_1 = 0.5, \tau = 10.0ms$, $t_1 = 40ms$, $t_2 = 300ms$, $c_1 = 80I/s$, $c_2 = 40I/s$ (cf. Fig. 1 C).

Now, that we have derived analytical expressions for the membrane potentials $\phi(x,t)$ we consider lines of equal potential defined by

$$\phi(x,t) = X(x)T(t) = \kappa = const\,. \quad (8)$$

This relation can either be solved for $x = x(t;\kappa)$ or $t = t(x;\kappa)$ giving the equipotential lines in parameterized form. Of particular interest is the case where κ equals the firing threshold ϑ (which is assumed to be the same for all cells; the exact form of the output-function above threshold does not matter at this point of the discussion). Then $x(t;\kappa)$ describes the time course of the boundary between silent (subthreshold) and firing (superthreshold) cells. This is equivalent to the width of the spatio-temporal receptive fields as observed in experiments by extracellular recordings of firing rates. Inserting $X(x)$ from (6) into (8) and isolating x we get

$$x^2(t) = 2\sigma_r^2 \ln\left[\frac{K_0\sigma_0\sigma_1}{\kappa\sigma_r}T(t)\right] \quad (9)$$

$$\overset{\sigma_1 \ll \sigma_0}{\approx} 2\sigma_0^2 \ln\left[\frac{K_0\sigma_1}{\kappa}T(t)\right]\,. \quad (10)$$

Using (7) for $T(t)$ we obtain the receptive field width for flashed stimuli. Example curves are plotted in Fig. 3 (left). Note that the width of the excited region closely resembles the experimental results although the width σ_r of the distribution of potentials is constant over time. The receptive field sharpening is explained by a decreasing region of cells above threshold (cf. discussion).

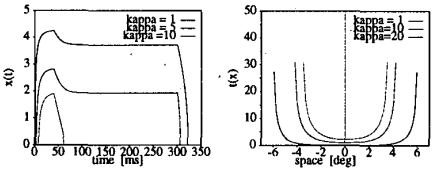

Fig.3: Width of the receptive field, $x(t)$ (left), and cortical firing latencies, $t(x)$ (right), for the regime $t_0 \leq t < t_1$, both for different values of κ. (Eqn. (10) also has a negative solution $-x(t)$, which is symmetric and left out for simplicity.)

Analogously, $t(x)$ can be determined. For $\kappa = \vartheta$ this defines the times, when cells at location x reach threshold, i.e. when they start or stop firing. Using (7) in the range $t_0 \leq t < t_1$ for $T(t)$, one finds for the cortical onset times

$$t(x) = -\tau \ln\left(1 - \frac{\kappa}{c_1 X(x)}\right) \quad (11)$$

$$\approx \frac{\kappa\tau}{c_1 X(x)} \approx \frac{\kappa\tau}{K_0 c_1 \sigma_1}\left(1 + \frac{x^2}{2\sigma_0^2}\right) \quad (12)$$

The approximations utilize Taylor expansions for $\ln(1-x)$ and $X(x)$ and are valid as long as $K_0 c_1 \sigma_1 \gg \kappa$, $x \ll \sigma_0$ and again $\sigma_1 \ll \sigma_0$. Eqn. (12) shows that the latencies increase quadratically with increasing distance x of the stimulus (spot) from the receptive field center (Fig. 3 right). A decrease of t can either be due to larger firing rates during LGN bursts c_1, a larger stimulus σ_1, or higher synpatic strengths K_0. The dependence on stimulus size should be testable in experiments. Firing rates of LGN-cells during Ca-bursts and synaptic strengths, however, are far more complicated to be controlled in experiments.

3 Experimental Data Fit

To test whether the model can accurately describe the experimental data and to estimate the model parameters, we fitted the analytical activation function derived in the previous section against experimental data. We used firing rates $\nu(x,t)$ of on- and corresponding off-subfields of 16 V1 cells recorded during both states of the EEG. Each field was sampled at 20 positions with .5 degree resolution and 30 time slices of 10 ms bin size (Fig. 4; for a detailed description of the experimental setup see [12]). Since the data were only sampled during stimulus presentation t_2 was fixed at 300 ms in the fit.

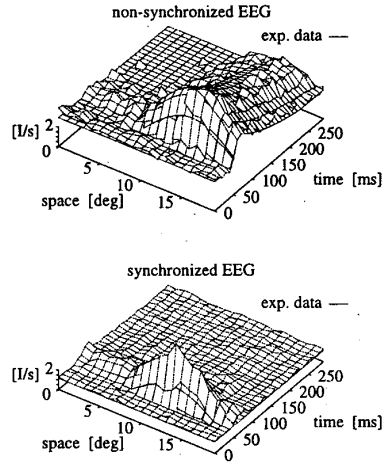

Fig.4: Top: Experimental spatio-temporal receptive field activity of an example cell during non-synchronized EEG. Bottom: Same cell during synchronized EEG. The tonic component is diminished.

The potentials $\phi(x,t)$ are supposed to transform into firing rates by means of a rectilinear function $f(\phi) = \beta[\phi - \vartheta]_+ + b$ [4] where b accounts for spontaneous background firing. Note, that $\phi(x,t)$ contains products of model parameters. This implies that we cannot determine all these parameters independently. For the same reason we may set β to unity. We determined the parameters of $\phi(x,t)$ by nonlinear least square fits (Levenberg-Marquardt [8]) of the data to the function

$$\nu(x,t) \stackrel{fit}{=} [X(x-a)T(t) - \vartheta]_+ + b \; . \quad (13)$$

For X we considered an (arbitrary) offset a of the receptive field center. From the fit, we can not directly obtain the parameters of the temporal LGN input c_i, but only the products $C_i := kc_i, i = 1,2$, with $k = K_0\sigma_0\sigma_1/\sigma_r$ (see Eqn. (6)).

For most subfields good fits were obtained (cf. Fig. 5). The mean standard deviation – calculated from the squared differences between fit and data – is of the same magnitude as the standard deviation of the baseline noise. In general, the fit is not as good for the receptive fields measured during synchronized EEG as during non-synchronized EEG. This is probably due to the missing tonic component.

The on-subfields in the non-synchronized case exhibited a significant adaptation during the tonic phase (cf. Fig. 5 right, 100–300 ms). In these cases an adaptation term was added to the fitting function (Eqn. (7)), i.e. c_2 was replaced by $c_2 exp(-(t-t_1)/\tau_a)$.

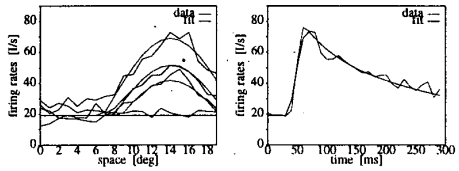

Fig.5: Model fit to an example data set (on-subfield during non-synchronized EEG). Left: Spatial fit for different times (0, 80, 140, 200 ms) Right: Temporal fit at a constant spatial position (the center of the Gaussian).

Comparing the parameters for on- and off-subfields in the two EEG states obtained from the fit, only few systematic dependences can be observed. The main difference is a delay of the off-subfields of approx. 20 ms ($t_0 = 43$ ms) compared to on-subfields ($t_0 = 21$ ms), which is in accordance with the literature [9, 5]. The main EEG state-dependence turns out to be the difference ΔC between C_1 and C_2, which is proportional to the difference of LGN activity during burst and during tonic phase (Fig. 6). ΔC is about twice as high in the synchronized (29 I/s) than in the non-synchronized state (16 I/s). Moreover, we find that bursts are more pronounced in the synchronized state (Fig. 6 left).

The burst duration instead seems to be state-independent and was on average 38 ms long. The difference between burst and tonic phase is mainly responsible for the restructuring of the receptive fields from wide to small. Somewhat surprisingly, we find

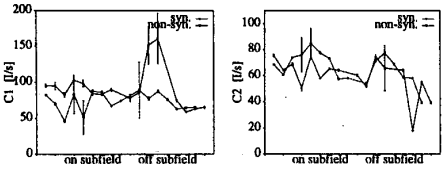

Fig.6: State-dependence of C_1 (left) which is proportional to the height of the burst component and C_2 (right) which is proportional to the height of the tonic component (cf. Eqn. (7)) as obtained from the fit to different on- and off-subfields. Some fits had to be excluded, since the cells had no off-subfield.

that the other model parameters do not exhibit dependences on EEG-state or on subfield type. Still, due the small overall standard deviations and due to the small standard deviations of the individual parameters (as calculated from the covariance matrix), it seems that our relatively simple approach is able to describe the dynamics in a statisfactory way.

For the remaining temporal parameters, we obtained $\tau = 13 \pm 7$ ms, $t_1 - t_0 = 38 \pm 17$ ms, $\tau_a = 541 \pm 238$ ms, which is in agreement with the literature [3, 10]. Although we used a pool-dynamic approach, a constant τ seems to be an adequate description, even for the different global states occuring in the experiment [12]. The spatial extension of the receptive field σ_r was on average 4.1 deg.

4 Conclusions

We have introduced a neural field model of LGN and V1 to describe EEG-dependent receptive field changes, which have recently been shown to exist in V1 [12]. The analytic expressions for the cortical spatio-temporal activity, Eqns. (6) and (7), show that this restructuring can be explained by state-dependent thalamic firing patterns (burst vs. tonic mode) and a pure feedforward mechanism. The restructuring is due to an 'iceberg' effect with a constant threshold θ: the potential distribution $\Phi(x,t) = X(x)T(t)$ consists of a spatial activity profile $X(x)$ with constant width, but a time- and state-dependent T. Therefore, the region of firing cells above threshold is time-dependent and sharpens with latency from stimulus onset. Hence, the sharpening should be ovservable in extracellular recordings of firing frequecies, but not in intracellular recordings of membrane potentials.

To test this hypothesis the model was fitted against experimental data. Here, it is most important that the fit is successful, although the width σ_r of the spatial profile of the estimated membrane potentials ϕ is constant over time. Also the firing thresholds ϑ is constant during the whole 300 ms response period, even though a strong modulation of the receptive field is present (as measured from spike rates). This supports the hypothesis that the experimentally observed receptive field changes are mainly due to changing input from LGN and not due to recurrent synaptic interactions in V1. Such intracortical circuits have been suggested to be responsible for the sharpening of orientation tuning curves [2, 10]. We neglected orientation effects in our model, but one should note that receptive field sharpening by recurrent intracortical processes would lead to changes in the width σ_r of $\phi(x,t)$ (similar to [2, 10]). In contrast, our model predicts a constant width. This difference between a feedforward and a feedback mechansim could be further investigated by intracellular recordings.

Based on this first analysis of single subfields, on- and off-fields will be added to the model to examine the influence of the restructuring on the interaction of different subfields.

References

[1] S.I. Amari. Dynamics of pattern formation in lateral-inhibition type neural fields. *Biol. Cybernetics*, 27:77–87, 1977.

[2] R. Ben-Yishai, R.L. Bar-Or, and H. Sompolinsky. Theory of orientation tuning in visual cortex. *Proc. Natl. Acad. Sci USA*, 92:3844–8, 1995.

[3] G.C. DeAngelis, I. Ohzawa, and R.D. Freeman. Receptive-field dynamics in the central visual pathway. *TINS*, 18:451–458, 1995.

[4] R.J. Douglas, C. Koch, M. Mahowald, K.A. Martin, and H.H. Suarez. Recurrent excitation in neocortical circuits. *Science*, 269(5226):981–5, 1995.

[5] K. Funke and F. Wörgötter. Differences in the temporal dynamics of the visual on and off pathways. *Exp. Brain Res.*, 104:171–176, 1995.

[6] G. Krone, H. Mallot, G. Palm, and A. Schüz. Spatiotemporal receptive fields: a dynamical model derived from cortical architectonics. *Proc. R. Soc. Lond.*, 226:421–444, 1986.

[7] P. Mineiro and D. Zipser. Analysis of direction selectivity arising from recurrent cortical interactions. *Neural Computation*, 10:353–371, 1998.

[8] W.H. Press, S.A. Teukolsky, W.T. Vetterling, and B.P. Flannery, editors. *Numerical Recipes in C: The Art of Scientific Computing.* Cambridge Univ. Press, 2 edition, 1993.

[9] P.H. Schiller. The on and off channels of the visual system. *TINS*, 15(3):86–91, 1992.

[10] D.C. Somers, S.B. Nelson, and M. Sur. An emergent model of orientation selectivity in cat visual cortical simple cells. *J. Neurosci.*, 15:5465–88, 1995.

[11] H.R. Wilson and J.D. Cowan. A mathematical theory of the functional dynamics of cortical and thalamic nervous tissue. *Kybernetik*, 13:55–80, 1973.

[12] F. Wörgötter, K. Suder, Y. Zhao, N. Kerscher, U. Eysel, and K. Funke. State-dependent receptive field restructuring in the visual cortex. *Nature*, 396(6707):165–168, 1998.